Journal of Materials Chemistry A

Accepted Manuscript

ROYAL SOCIETY OF CHEMISTRY

www.rsc.org/materialsA

Journal Name

ARTICLE

NiO nanosheets as efficient top hole transporters for carbon counter electrode based perovskite solar cells

Received 00th January 20xx,
Accepted 00th January 20xx

DOI: 10.1039/x0xx00000x

www.rsc.org/

Zonghao Liu, ‡[a] Meng Zhang, ‡[a] Xiaobao Xu,[a] Fensha Cai,[a] Huailiang Yuan,[a] Lingling Bu,[a] Wenhui Li,[a] Aili Zhu,[a] Zhixin Zhao,*[a] Mingkui Wang,*[a] Yi-Bing Cheng,[ac] Hongshan He*[b]

Here, we present fully printable carbon electrode based perovskite solar cells using highly crystalline NiO nanosheets as a top hole transport layer, mesoporous TiO_2 nanoparticles as a bottom electron transport layer and ZrO_2 as an intermediate spacer layer, respectively. Time-resolved photoluminescence decay measurements, electronic impedance spectroscopy and transient photovoltage decay measurements have revealed that the NiO nanosheets as top hole tranporters exhibit superior charge collection efficiency and a prolonged charge lifetime. As a result, the impressive power conversion efficiency of 14.2% is achieved under standard testing conditions.

Introduction

Solution-processable organic-inorganic lead halide perovskite materials, such as $CH_3NH_3PbX_3$ (X = Cl, Br, I), have shown great promise for low-cost thin film solar cells. During the last three years, extensive efforts have been devoted to the development of efficient fabrication technologies with energy conversion efficiency over 20% being achieved recently[1] due to strong light absorption, suitable direct optical band gap, weak excitons binding energy, large electron and hole mobility, and long electron diffusion length of perovskites.[2-5] However, the state-of-the-art PVSCs require organic hole transport materials and noble metal for proper operation. [6] For example, the top charge transport layer used in perovskite cells (PVSCs) is usually organic materials, such as PCBM and spiro-OMeTAD,[7,8] which possess several unfavourable properties, such as poor crystallinity, low mobility, possible degradation and high cost. Recently, inorganic materials such as CuSCN[9-12] and CuI[13] have been used successfully as hole selective materials; however, the overall performance of the resulting devices is poor.[6]

Nickel oxide (NiO)[7,11,14-18] has been used as a hole transporter in PVSCs successfully. Like several other nanostructured oxide materials including nanorod,[19] nanofiber[20] and core-shell,[21] nanowire,[22] nickel oxide can efficiently enhance charge extraction and prolong the charge lifetime. [23,24] More importantly, NiO exhibits much better thermal and chemical stability than spiro-OMeTAD, which is favourable to the long stability of PVSCs.[26,27] Contrary to spiro-OMeTAD that requires multi-step organic synthesis and tedious purification,[25,26] NiO is abundant and can be prepared by simple and low-cost synthetic processes. When combined with other carbon materials, such as carbon/graphite composite,[28-31] carbon nanotube,[32,33] graphene,[34] carbon ink,[35] and commercial carbon paste,[36,37] the resulting devices offer great potential for fully printable and cost-effective devices without using expensive Au and Ag.[33,34]. Unfortunately, the photovoltaics performance of fabricated devices is inferior to state-of-the-art devices and significant improvement is needed.

Our previous study showed that NiO nanoparticles improved the charge collection efficiency compared to ZrO_2 nanoparticles in carbon/graphite counter electrode-based PVSCs. [23] In these devices, NiO nanoparticles were deposited directly on the top of TiO_2 nanoparticle layer, which could cause anomalous recombination leading to poor energy conversion efficiency.[24] We reported here a new strategy to address this concern. We apply highly crystalline NiO nanosheets as a top nanostructured charge transport layer by inserting an additional ZrO_2 layer between TiO_2 layer and NiO layer. The resulting films exhibit superior charge collection efficiency and a prolonged charge lifetime. The resulting devices exhibit impressive energy conversion efficiency of 14.2% under AM 1.5G conditions.

[a] Michael Grätzel Center for Mesoscopic Solar Cells, Wuhan National Laboratory for Optoelectronics, School of Optical and Electronic Information, Huazhong University of Science and Technology, Wuhan, Hubei 430074, PR China, E-mail: mingkui.wang@mail.hust.edu.cn, zhixin-zhao@hust.edu.cn; Fax: +86 27 87792225; Tel: + 86 27 87793867
[b] Department of Chemistry, Eastern Illinois University, Charleston, Illinois 61920, United States; Email: hhe@eiu.edu; Tel:01-217-581-6231
[c] Department of Materials Engineering, Monash University, Melbourne, Victoria 3800, Australia.
‡These authors contributed equally to this work.
Electronic Supplementary Information (ESI) available: [EDX spectra of NiO nanosheet based devices, devices performance distribution, equivalent circuit and EIS data of devices, BET of NiO powder, transient photovoltage decay measurements data of devices.]. See DOI: 10.1039/x0xx00000x

Experimental

Synthesis of NiO nanosheets.

Firstly, 0.582 g nickel (II) nitrate hexahydrate was dissolved in 100 mL distilled water, and then transferred into a three-neck flask. Then, an aqueous solution (50 mL) of 4 mM oxalic acid dihydrate and 20 mM hexamethylenetetramine were added dropwise under stirring in 30 min. The resulting mixture was heated to 100 ^{o}C and refluxed for 6 hours. The green precipitate was collected by filtration and washed with water and ethanol three times. After drying at 60 ^{o}C in a vacuum chamber for 12 h, the green product was heated in a muffle furnace in air at 400 ^{o}C for 2 hours to give a fine grey NiO nanosheets powder. Screen printing NiO nanosheets paste were prepared by mixing ethyl cellulose solution in ethanol (44 wt%), terpineol (46 wt%) and NiO nanosheets powder (10 wt%), followed by ultrasonication and vigorous stirring. After well dispersed, ethanol was removed by rotary evaporation.

Device fabrication.

The devices were fabricated as we described previously.[23] FTO conducting glass were etched with sander to form two detached electrode patterns before being ultrasonically cleaned with detergent solution, deionized water and ethanol successively. A compact TiO_2 layer was deposited on the cleaned FTO glass by spray pyrolysis deposition with di-isopropoxytitanium bis(acetyl acetonate) solution at 450 ^{o}C. The films were sintered at 500 ^{o}C for 30 min and then cooled to room temperature. A 450 nm mesoporous TiO_2 (DSL. 18NR-T, 20 nm, Dyesol, Australia, diluted at 1/3.5 mass ratio of paste/terpineol) layer, a 400 nm ZrO_2 spacer layer, 1 µm NiO layer and a 8 µm carbon black/graphite layer were subsequently prepared by screen printing onto FTO conducting glass layer by layer, which were sintered at 500 ^{o}C, 500 ^{o}C, 500 ^{o}C and 400 ^{o}C for 30 min respectively. The obtained films were then infiltrated with PbI_2 by dropping a PbI_2 solution in DMF (462 mg mL^{-1}) that was kept at 70 ^{o}C. After drying, the films were dipped into 2-propanol for 1-2 s before being dipped in a solution of CH_3NH_3I in 2-propanol (10 mg mL^{-1}) for 10 min and then rinsed with 2-propanol. The films changed colour from light yellow to black during the dipping process, indicating the formation of the perovskite $CH_3NH_3PbI_3$. After annealing at 70 ^{o}C for 30 min, the fabrication of the device was finished. All the procedures above were completed in dry air atmosphere.

Characterization.

The crystal phases of NiO nanosheets were identified by X-ray powder diffraction (XRD, X'Pert PRO, Cu Kα radiation, Panalytical B. V.). The morphology of NiO nanosheets was observed using a field emission scanning electron microscope (FE-SEM, Nova NanoSEM), and a transmission electron microscope (TEM, Tecnai G2 20, FEI). Brunauer-Emmett-Teller (BET) analysis was used to determine the surface area and the pore size distribution, on an ASAP 2020 accelerated surface area and porosimetry analyzer. The thickness of mesoscopic layer was confirmed by a commercial profiler (DEKTAK 150, VECCO, Bruker).

A Xenon light source solar simulator (450 W, Oriel, model 9119) with an AM 1.5G filter (Oriel, model 91192) was used to give an irradiance of 100 mW cm^{-2} at the surface of the solar cells. The current-voltage characteristics of the devices under these conditions were obtained by applying external potential bias to the devices and measuring the generated photocurrent with a Keithley model 2400 digital source meter. A similar data acquisition system was used to control the incident photon-to-current conversion efficiency (IPCE) measurement. The devices (~0.6 cm^2) were tested using a metal mask to prevent the scattering light.

Electronic impedance spectroscopy (EIS) was carried out on a Zennium electrochemical workstation (Zahner 6.0, Germany) in the frequency range from 100 mHz to 1 MHz with 10 mV AC amplitude under the LED simulated light. The electron lifetime was determined by transient photovoltage decay measurements. An array of diodes was used to produce a white light bias and blue-light diodes controlled by a fast solid-state switch to generate a pulse (0.05 s square pulse-width, 100 ns rise and fall time). The voltage dynamics were recorded on a digital oscilloscope (Tektronix MDO3032). By varying the intensity of the white-light bias, the recombination rate constant and the electron diffusion rate constant could be estimated over a range of applied biases.

Results and Discussion

The NiO nanosheets were characterized by TEM and XRD, as shown in Fig. 1. The NiO nanosheet exhibits a hierarchical structure of porous flower with a diameter of ~1.5 µm as shown in Fig. 1a-c. It can be seen from Fig. 1d that the peak positions appearing at 2θ = 37.14°, 43.29°, 62.80°, 75.38°, 79.31° can be indexed at (111), (200), (220), (311), and (222) crystal planes of the NiO, respectively, indicating that the as-synthesized NiO nanosheets is cubic NiO. The NiO lattice constant calculated from the XRD data is 4.2164 Å, which is in good agreement with the reported data. [38,39]

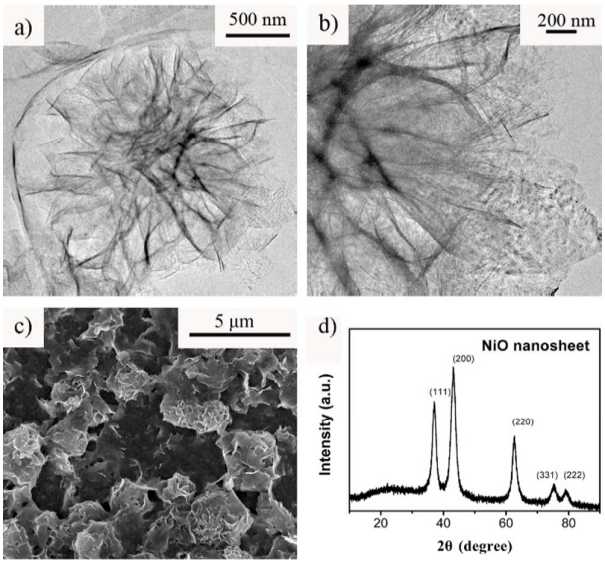

Fig. 1 TEM images (a, b), SEM image (c) and XRD pattern (d) of the NiO nanosheets.

Time-resolved photoluminescence (TRPL) decay measurements were performed to evaluate the charge transfer at the $CH_3NH_3PbI_3$/NiO nanosheets (NiO-NS) interface. The result is shown Fig. 2. For comparison purpose, the samples of $CH_3NH_3PbI_3$/NiO

nanoparticles (NiO-NP) and $CH_3NH_3PbI_3/ZrO_2$ nanoparticle (ZrO_2-NP) are also measured and presented in Fig. 2. The normalized TRPL decay shows that both $CH_3NH_3PbI_3$/NiO-NP and $CH_3NH_3PbI_3$/NiO-NS samples exhibit faster quenching relative to the $CH_3NH_3PbI_3/ZrO_2$ sample, indicating a fast charge transfer from $CH_3NH_3PbI_3$ to NiO after photon excitation.[40] Moreover, the NiO NS exhibits a PL lifetime (τ_e) of 2.4 ns, which is shorter than the PL lifetime of NiO NP (5.1 ns), indicating that the nanosheet could be acting as more effective hole collector in comparison to nanoparticles. This result could be caused by the efficient interfacial contact between $CH_3NH_3PbI_3$ and NiO NS.[38,41,42]

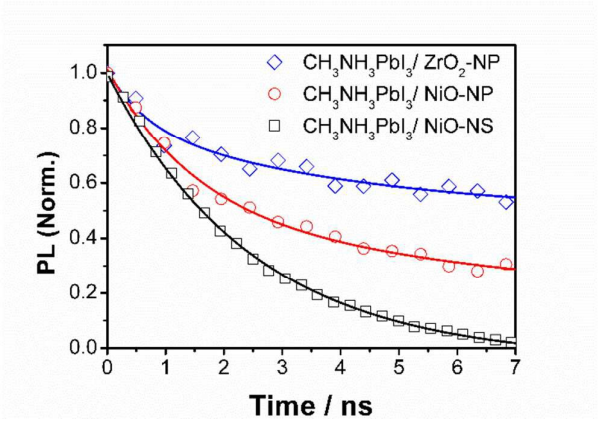

Fig. 2 Time-resolved photoluminescence decays of $CH_3NH_3PbI_3$/NiO-NP film (red circle), $CH_3NH_3PbI_3$/NiO-NS film (black square), $CH_3NH_3PbI_3/ZrO_2$-NP film (blue diamond). Excitation wavelength: 443 nm.

Fig. 3a shows the schematic of a typical carbon counter electrode based PVSC device using NiO nanosheets as an top hole collector. In such devices, a compact TiO_2 nanoparticles, mesoporous TiO_2 nanoparticles, ZrO_2 nanoparticles, NiO nanosheets and carbon/graphite are used as an hole blocking layer, a bottom electron transport layer, an intermediate insulation layer, a top hole transport layer and a counter electrode, respectively. Fig. 3b shows the cross sectional SEM image of the interfacial junction structure of active layers in the device. The $CH_3NH_3PbI_3$, fully infiltrated inside of TiO_2, ZrO_2 and NiO layers, injects electron into the conduction band of TiO_2,[8] and hole into the valence band of NiO [16,40], respectively. Both electron and hole transfer inside ZrO_2 layer due to their large electron and hole mobility and conductivity.[3,43-45] Furthermore, ZrO_2 layer is believed to separate the TiO_2 layer and the NiO layer to suppress interfacial charge recombination.[24] The $CH_3NH_3PbI_3$ light absorption materials was deposited with two-step deposition method inside of the entire mesoporous layers with uniform distribution. This was confirmed by the EDX spectra as shown in Fig. S1. Compared to the NiO nanoparticle, it is difficult to prepare very thin films without losing continuity of the film. Therefore, the thickness of NiO nanosheet layer was set to 1 µm in this study, which was also the limit we could achieve in the laboratory. To ensure comparison is meaningful, NiO nanoparticles with the same thickness (1 µm) were used to exclude the thickness effects on photovoltaic performance. In this way, other effects including pore filling, crystallinity and interface on charge collection and charge recombination will be easily clarified. It's also worth noting that the 1 µm film thickness is not the optimized thickness for NiO nanoparticle based device.

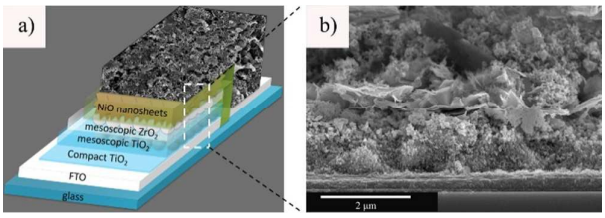

Fig. 3 a) The schematic of a typical carbon counter electrode based perovskite solar cells device using NiO nanosheets as an hole collector. **b)** Cross sectional SEM image of the active layers interfacial junction structure of the device.

Fig. 4a shows the current density-voltage (*J-V*) curves for the NiO-NP based and NiO-NS based PVSC devices measured under simulated AM 1.5 (100 mW cm^{-2}). The histogram of power conversion efficiency was shown in Fig. S2. The NiO-NP based PVSC exhibited the highest PCE of 12.4% with a J_{SC} of 19.5 mA cm^{-2}. The NiO-NS based PVSC device exhibits an increased PCE of 14.2% with a J_{SC} of 20.4 mA cm^{-2} and a V_{OC} of 965 mV. Fig. 4b shows the IPCE spectra of the devices in the range from 300 nm to 850 nm. The NiO-NS device exhibits higher IPCE value than that of NiO-NP device. An effective charge collection property of NiO-NS is believed to contribute significantly to the increased voltage and current in NiO-NS based devices than that with a NiO-NP layer. An anomalous hysteresis often has been observed in perovskite solar cells with different device architecture.[46,47] As shown in Fig. 5a, we also compared the forward bias to short circuit (FB-SC) and short-circuit to forward bias (SV-FB) *J*-V curves of NiO nanosheets solar cells. There is negligible hysteresis was observed in such devices, which is ascribed to effective charge extraction from $CH_3NH_3PbI_3$ to oxide nanomaterials when considering the device architecture.[48,49] The steady-state power output at a forward bias of 0.7 V as a function of time was carried out to understanding the stabilized power output under working conditions.[46] As shown in Fig. 5b, the photocurrent density stabilizes within seconds to approximately 20.0 mA cm^{-2}, yielding the stabilized power conversion efficiency around 13.9% measured after 100 s. This indicates that the test conditions provide an accurate representation of the device photovoltaic performance.

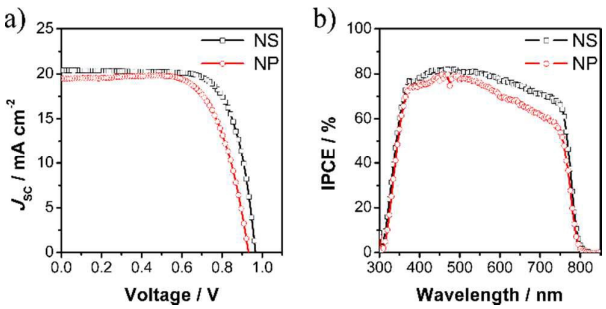

Fig. 4 a) Current-Voltage (*J-V*) characteristics of NiO-NS based perovskite solar cells (NS, black square) and NiO-NP based perovskite solar cells (NP, red circle) under simulated AM 1.5 (100 mW cm^{-2}) condition. **b)** The IPCE spectra of NiO-NS based perovskite solar cells (NS, black square) and NiO-NP based perovskite solar cells (NP, red circle).

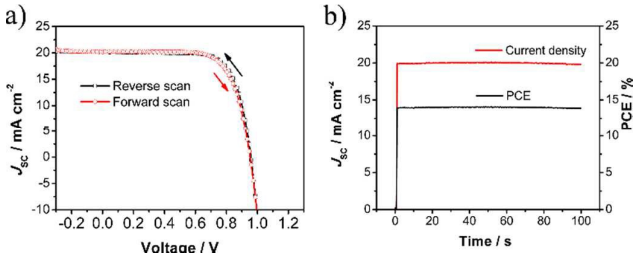

Fig. 5 a) Current-voltage curves with forward bias to short circuit (reverse scan, from 1.0 V to -0.3 V, black) and from short circuit to forward bias (forward scan, from -0.3 V to 1.0 V, red) for NiO nanosheets based device measured under simulated AM 1.5 (100 mW cm^{-2}) sunlight at scan rate of 0.05V/s. **b)** Current density and Power conversion efficiency (PCE) as a function of time for the NiO nanosheets based device held at a forward bias of maximum output power point (0.70 V). The device was placed in the dark prior to the start of the measurement.

Table 1. Device performance of the NiO nanosheets based device (NiO-NS) and the NiO nanoparticle (NiO-NP) device measured under simulated AM 1.5 (100 mW cm^{-2}) conditions.

device	J_{SC}(mA cm^{-2})	V_{OC}(mV)	FF	η (%)
NiO-NS	20.4	965	0.72	14.2
NiO-NP	19.5	930	0.68	12.4

EIS measurements were conducted to investigate the internal properties of PVSCs. Fig. 6 shows the Nyquist plots of devices using NiO-NP or NiO-NS under illumination at bias of 0.7 V. The Nyquist plots of the devices show three main features: (i) an arc at high frequencies region attributed to the charge exchange process at the counter electrode interface, (ii) an arc at middle frequencies region attributed to the charge recombination process at the perovskite/NiO interface, (iii) an arc at low frequencies represents a slow process correlating to ionic motion in perovskite.[50-52] Here, we use three lumped RC-circuit in series as shown in Fig. 6 (inset) to fit the impedance data. Since the NiO-NS and NiO-NP devices contain the same TiO_2/perovskite interface, the difference in the mediate frequencies region is dominated by the perovskite/NiO interface.

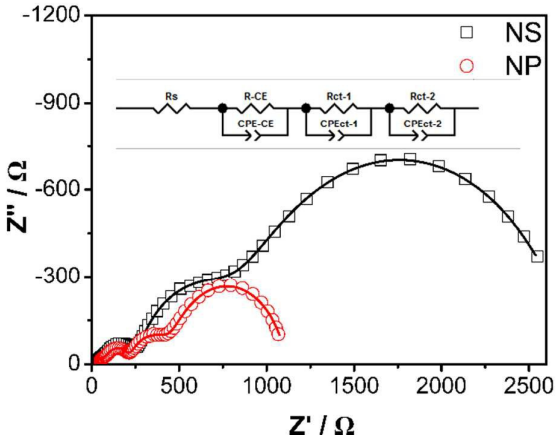

Fig. 6 Electrical impedance spectroscopy characterization. Nyquist plots of NiO nanosheets device (NS, black square) and NiO nanoparticle device (NP, red circle) measured under light 10 mW cm^{-2} with bias at 0.7 V. The solid line are the fitted curves. Inset: the equivalent circuit for fitting the EIS data.

The R_{ct} 1 and τ_e 1 obtained from EIS at different bias are shown in Fig. 7 and the corresponding capacitance C1 are shown in Fig. S3. The Fig. 7a indicates that the NiO-NS device exhibits relatively larger charge recombination resistance (R_{ct} 1) than that of NiO-NP device. Fig. 7b shows the calculated lifetime τ_e 1 (τ_e 1 = R_{ct} 1•C 1) as a function of the applied bias[24,50,53] under different bias for NS and NP-based cells. NS-based devices exhibit longer electron lifetimes that NS-based cells signifying the NiO-NS device also has longer charge recombination lifetime. These results imply that the highly crystalline of NiO nanosheets have less surface defects, which reduces charge recombination probability.[42]

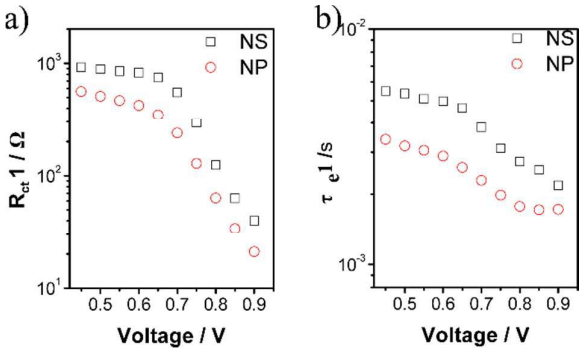

Fig. 7 a) Plot of charge recombination resistance (R_{ct} 1) and b) charge recombination lifetime τ_e 1 at the NiO/perovskite interface obtained from impedance measurements under illumination at given bias for NiO-NS device (NS, black square) and NiO-NP devices (NP, red circle).

Fig. 8a presents the low frequency resistance obtained from impedance measurement. The corresponding time constant τ_e 2 calculated from R_{ct}2 and C2 within a hundred to thousand millisecond time scale is shown in Fig. 8b, corresponding to ion motion in the perovskite.[51,56-58] The small differences in τ_e 2 for the two devices implies the observation of device photovoltaic performance is not related to this element. Transient photovoltage decay measurements were carried out to determine the interfacial charge recombination of the two devices. As shown in Fig. S6, NiO-NS device shows a longer lifetime than that of NiO-NP device, indicating more efficient hole extraction and charge separation as discussed above.

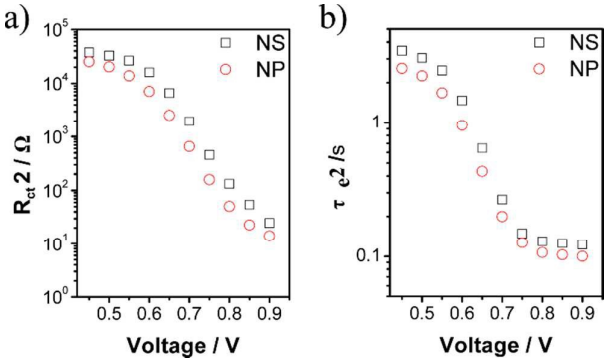

Fig. 8 a) Plot of transport resistance (R_{ct} 2) and b) time constant τ_e 2 corresponding to the ion motion in perovskite in NiO nanosheets device (NS, black square) and NiO nanoparticle device (NP, red circle) obtained from impedance measurements under illumination at given bias.

Though the NiO-NS films showed lower surface area than NiO-NP film, the NiO-NS based device have better performance. This can be

attributed to better pore filling, better perovskite crystallinity, and suitable NiO surface. The BET results in Table S1 and Fig. S4 show that the NiO-NS film has larger pore size than that of NiO-NP film. Therefore, the perovskite can easily infiltrate from the top to the bottom mesoporous electrode in NiO-NS films. This benefits the pore filling of the perovskite. In addition, larger perovskite grains should form in the pore of NiO-NS, reducing the probability of charge recombination.[54,55] As the PL decay study confirmed that the effective charge transfer dominates device performance rather than the apparent mesoporous electrode surface area. This clearly indicates the favourable perovskite/NiO interfaces for charge extraction in NiO-NS films. The counter electrode interfaces also affected the device performance. As shown in Fig. S5, the NiO-NS device exhibits relatively smaller charge transfer resistance (R_{CE}) than that of NiO-NP device. This may be due to the better electrical contact of the three components at the counter electrode interface, which enhances the charge collection at this interface. As a result of aforementioned effects, the employment of NiO nanosheets as an efficient hole conductor facilitating hole extraction, and retarding the charge recombination, resulted in a 30 mV higher V_{OC} and 1 mA cm^{-2} higher J_{SC}.

Carbon based PVSC devices have been proven to possess good thermal stability than conventional cells with metal back contact.[29,59] We also conducted long-term stability testing on NiO-NS PVSC. After capsulated under N_2 in glove box, the sealed devices were subjected to constant light illumination with light density of 75 mW cm^{-2} at 50 °C. Fig. 9 shows the normalized PCE as a function of storage time. The device still showed 60 % of the initial highest PCE after light soaking for 250 hours at 50 °C. During the testing, the photocurrent dropped quickly at the first 50 hours. The relatively good stability of this type solar cell may be attributed to the hydrophobic property of carbon materials and a thick perovskite layer used, which might induce a slow degradation.[60] Nevertheless, the stability of perovskite solar cells is still a major concern for future practical applications.

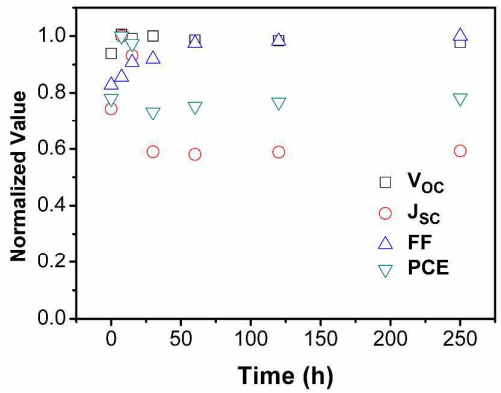

Fig. 9 The normalized photovoltaic parameters of capsulated NiO nanosheets based devices under illumination with light density of 75mW cm^{-2} at 50 °C.

Conclusions

In summary, we demonstrated a carbon electrode based perovskite solar cells utilizing highly crystalline NiO nanosheets as a top hole transport layer. The NiO nanosheets provides superior charge collection and prolonged charge lifetime, resulting in a 15% increase of energy conversion efficiency compared to the NiO nanoparticle based devices, and achieving a cell with impressive energy conversion efficiency of 14.2% under AM 1.5G conditions. To our best knowledge, this was the first report of nanostructure optimization for the top charge transport layer in perovskite solar cells. We suggest that an efficient nanostructured top charge conductor can further enhance the photovoltaic performance of perovskite solar cells.

Acknowledgements

This work was partially supported by the National Basic Research Program of China (973 program 2011CBA00703), the Fundamental Research Funds for the Central Universities (grant no. HUST: 2014TS016) and Director Fund of Wuhan National Laboratory for Optoelectronics (ZZ), NSFC (21103057), the CME with the Program of New Century Excellent Talents in University (NCET-10-0416) (WM), and Council on Faculty Research, and the President's Fund for Research and Creative Activity, Eastern Illinois University (HH). We thank the Analytical and Testing Center of Huazhong University of Science and Technology for XRD, SEM and TEM testing.

Notes and references

(1) Yang, W. S.; Noh, J. H.; Jeon, N. J.; Kim, Y. C.; Ryu, S.; Seo, J.; Seok, S. I. *Science* **2015**, *348*, 1234-1237.

(2) Roiati, V.; Colella, S.; Lerario, G.; De Marco, L.; Rizzo, A.; Listorti, A.; Gigli, G. *Energy Environ. Sci.* **2014**, *7*, 1889-1894.

(3) Xing, G.; Mathews, N.; Sun, S.; Lim, S. S.; Lam, Y. M.; Grätzel, M.; Mhaisalkar, S.; Sum, T. C. *Science* **2013**, *342*, 344-347.

(4) Hodes, G. *Science* **2013**, *342*, 6156.

(5) Green, M. A.; Ho-Baillie, A.; Snaith, H. J. *Nat. Photonics.* **2014**, *8*, 506–514.

(6) Li, M.; Shen, P.; Wang, K.; Guo, T.; Chen, P. *J. Mater. Chem. A* **2015**.

(7) Jeng, J.; Chen, K.; Chiang, T.; Lin, P.; Tsai, T.; Chang, Y.; Guo, T.; Chen, P.; Wen, T.; Hsu, Y. *Adv. Mater.* **2014**, *26*, 4107–4113.

(8) Kim, H.; Lee, C.; Im, J.; Lee, K.; Moehl, T.; Marchioro, A.; Moon, S.; Humphry-Baker, R.; Yum, J.; Moser, J. E.; Grätzel, M.; Park, N. *Sci. Rep.* **2012**, *2*, 259.

(9) Qin, P.; Tanaka, S.; Ito, S.; Tetreault, N.; Manabe, K.; Nishino, H.; Nazeeruddin, M. K.; Grätzel, M. *Nat. Commun.* **2014**, *5*, 3834.

(10) Ito, S.; Tanaka, S.; Vahlman, H.; Nishino, H.; Manabe, K.; Lund, P. *ChemPhysChem* **2014**, *15*, 1194–1200.

(11) Subbiah, A. S.; Halder, A.; Ghosh, S.; Mahuli, N.; Hodes, G.; Sarkar, S. K. *J. Phys. Chem. Lett.* **2014**, *5*, 1748–1753.

(12) Ito, S.; Tanaka, S.; Manabe, K.; Nishino, H. *J. Phys. Chem. C* **2014**, *118*, 16995–17000.

(13) Christians, J. A.; Fung, R. C. M.; Kamat, P. V. *J. Am. Chem. Soc.* **2014**, *136*, 758–764.

(14) Hu, L.; Peng, J.; Wang, W.; Xia, Z.; Yuan, J.; Lu, J.; Huang, X.; Ma, W.; Song, H.; Chen, W.; Cheng, Y.; Tang, J. *ACS Photonics* **2014**, *1*, 547–553.

(15) Wang, K.; Shen, P.; Li, M.; Chen, S.; Lin, M.; Chen, P.; Guo, T. *ACS Appl. Mater. Interfaces* **2014**, *6*, 11851–11858.

(16) Wang, K.; Jeng, J.; Shen, P.; Chang, Y.; Diau, E. W.; Tsai, C.; Chao, T.; Hsu, H.; Lin, P.; Chen, P.; Guo, T.; Wen, T. *Sci. Rep.*

2014, *4*, 4756.

(17) Tian, H.; Xu, B.; Chen, H.; Johansson, E. M. J.; Boschloo, G. *ChemSusChem* **2014**, *7*, 2150–2153.

(18) Cui, J.; Meng, F.; Zhang, H.; Cao, K.; Yuan, H.; Cheng, Y.; Huang, F.; Wang, M. *ACS Appl. Mater. Interfaces* **2014**, *6*, 22862-22870.

(19) Son, D.; Im, J.; Kim, H.; Park, N. *J. Phys. Chem. C* **2014**, *118*, 16567-16573.

(20) Dharani, S.; Mulmudi, H. K.; Yantara, N.; Thu Trang, P. T.; Park, N. G.; Graetzel, M.; Mhaisalkar, S.; Mathews, N.; Boix, P. P. *Nanoscale* **2014**, *6*, 1675-1679.

(21) Zhang, W.; Saliba, M.; Stranks, S. D.; Sun, Y.; Shi, X.; Wiesner, U.; Snaith, H. J. *Nano Lett.* **2013**, *13*, 4505-4510.

(22) Im, J.; Luo, J.; Franckevičius, M.; Pellet, N.; Gao, P.; Moehl, T.; Zakeeruddin, S. M.; Nazeeruddin, M. K.; Grätzel, M.; Park, N. *Nano Lett.* **2015**, *15*, 2120-2126.

(23) Liu, Z.; Zhang, M.; Xu, X.; Bu, L.; Zhang, W.; Li, W.; Zhao, Z.; Wang, M.; Cheng, Y.; He, H. *Dalton Trans.* **2015**, *44*, 3967-3973.

(24) Xu, X.; Liu, Z.; Zuo, Z.; Zhang, M.; Zhao, Z.; Shen, Y.; Zhou, H.; Chen, Q.; Yang, Y.; Wang, M. *Nano Lett.* **2015**, *15*, 2402-2408.

(25) Salbeck, J.; Yu, N.; Bauer, J.; Weiss Rtel, F.; Bestgen, H. *Synth. Met.* **1997**, *91*, 209-215.

(26) Odobel, F.; Le Pleux, L.; Pellegrin, Y.; Blart, E. *Acc. Chem. Res.* **2010**, *43*, 1063–1071.

(27) Chen, Q.; De Marco, N.; Yang, Y. M.; Song, T.; Chen, C.; Zhao, H.; Hong, Z.; Zhou, H.; Yang, Y. *Nano Today* **2015,** Doi:10.1016/j.nantod.2015.04.009.

(28) Ku, Z.; Rong, Y.; Xu, M.; Liu, T.; Han, H. *Sci. Rep.* **2013**, *3*, 3132.

(29) Mei, A.; Li, X.; Liu, L.; Ku, Z.; Liu, T.; Rong, Y.; Xu, M.; Hu, M.; Chen, J.; Yang, Y.; Grätzel, M.; Han, H. *Science* **2014**, *345*, 6194.

(30) Hu, M.; Liu, L.; Mei, A.; Yang, Y.; Liu, T.; Han, H. *J. Mater. Chem. A* **2014**, *2*, 17115-17121.

(31) Liu, L.; Mei, A.; Liu, T.; Jiang, P.; Sheng, Y.; Zhang, L.; Han, H. *J. Am. Chem. Soc.* **2015**, *137*, 1790-1793.

(32) Li, Z.; Kulkarni, S. A.; Boix, P. P.; Shi, E.; Cao, A.; Fu, K.; Batabyal, S. K.; Zhang, J.; Xiong, Q.; Wong, L. H.; Mathews, N.; Mhaisalkar, S. G. *ACS Nano* **2014**, *8*, 6797-6804.

(33) Wang, X.; Li, Z.; Xu, W.; Kulkarni, S. A.; Batabyal, S. K.; Zhang, S.; Cao, A.; Wong, L. H. *Nano Energy* **2015**, *11*, 728-735.

(34) Yan, K.; Wei, Z.; Li, J.; Chen, H.; Yi, Y.; Zheng, X.; Long, X.; Wang, Z.; Wang, J.; Xu, J.; Yang, S. *Small* **2015**, *11*, 2269–2274.

(35) Wei, Z.; Chen, H.; Yan, K.; Yang, S. *Angew. Chem. Int. Ed.* **2014**, *53*, 13239-13243.

(36) Zhang, F.; Yang, X.; Wang, H.; Cheng, M.; Zhao, J.; Sun, L. *ACS Appl. Mater. Interfaces* **2014**, *6*, 16140-16146.

(37) Zhou, H.; Shi, Y.; Dong, Q.; Zhang, H.; Xing, Y.; Wang, K.; Du, Y.; Ma, T. *J. Phys. Chem. Lett.* **2014**, *5*, 3241-3246.

(38) Powar, S.; Wu, Q.; Weidelener, M.; Nattestad, A.; Hu, Z.; Mishra, A.; Bäuerle, P.; Spiccia, L.; Cheng, Y.; Bach, U. *Energy Environ. Sci.* **2012**, *5*, 8896-8900.

(39) Xiong, J.; Shen, H.; Mao, J.; Qin, X.; Xiao, P.; Wang, X.; Wu, Q.; Hu, Z. *J. Mater. Chem.* **2012**, *22*, 11927-11932.

(40) Hsu, H.; Wang, C.; Fathi, A.; Shiu, J.; Chung, C.; Shen, P.; Guo, T.; Chen, P.; Lee, Y.; Diau, E. W. *Angew. Chem. Int. Ed.* **2014**, *53*, 9339–9342.

(41) Zhu, Z.; Bai, Y.; Zhang, T.; Liu, Z.; Long, X.; Wei, Z.; Wang, Z.; Zhang, L.; Wang, J.; Yan, F.; Yang, S. *Angew. Chem. Int. Ed.* **2014**, *53*, 12571–12575.

(42) Zhang, X. L.; Huang, F.; Nattestad, A.; Wang, K.; Fu, D.; Mishra, A.; Bäuerle, P.; Bach, U.; Cheng, Y. *Chem. Commun.* **2011**, *47*, 4808.

(43) Lee, M. M.; Teuscher, J.; Miyasaka, T.; Murakami, T. N.; Snaith, H. J. *Science* **2012**, *338*, 643-647.

(44) Stranks, S. D.; Eperon, G. E.; Grancini, G.; Menelaou, C.; Alcocer, M. J. P.; Leijtens, T.; Herz, L. M.; Petrozza, A.; Snaith, H. J. *Science* **2013**, *342*, 341-344.

(45) Dong, Q.; Fang, Y.; Shao, Y.; Mulligan, P.; Jie Qiu, L. C.; Huang, J. *Science* **2015**, *347*, 967-970.

(46) Snaith, H. J.; Abate, A.; Ball, J. M.; Eperon, G. E.; Leijtens, T.; Noel, N. K.; Stranks, S. D.; Wang, J. T.; Wojciechowski, K.; Zhang, W. *J. Phys. Chem. Lett.* **2014**, *5*, 1511-1515.

(47) Kim, H.; Park, N. *J. Phys. Chem. Lett.* **2014**, *5*, 2927-2934.

(48) Chen, H.; Sakai, N.; Ikegami, M.; Miyasaka, T. *J. Phys. Chem. Lett.* **2015**, *6*, 164-169.

(49) Wei, J.; Zhao, Y.; Li, H.; Li, G.; Pan, J.; Xu, D.; Zhao, Q.; Yu, D. *J. Phys. Chem. Lett.* **2014**, *5*, 3937-3945.

(50) Guillén, E.; Ramos, F. J.; Anta, J. A.; Ahmad, S. *J. Phys. Chem. C* **2014**, *118*, 22913-22922.

(51) Kim, H.; Mora-Sero, I.; Gonzalez-Pedro, V.; Fabregat-Santiago, F.; Juarez-Perez, E. J.; Park, N.; Bisquert, J. *Nat. Commun.* **2013**, *4*, 2242-2248.

(52) Dualeh, A.; Moehl, T.; Tétreault, N.; Teuscher, J.; Gao, P.; Nazeeruddin, M. K.; Grätzel, M. *ACS Nano* **2014**, *8*, 362–373.

(53) Wang, M.; Chen, P.; Humphry-Baker, R.; Zakeeruddin, S. M.; Grätzel, M. *ChemPhysChem* **2009**, *10*, 290-299.

(54) Xiao, Z.; Dong, Q.; Bi, C.; Shao, Y.; Yuan, Y.; Huang, J. *Adv. Mater.* **2014**, *26*, 6503-6509.

(55) Nie, W.; Tsai, H.; Asadpour, R.; Blancon, J. C.; Neukirch, A. J.; Gupta, G.; Crochet, J. J.; Chhowalla, M.; Tretiak, S.; Alam, M. A.; Wang, H. L.; Mohite, A. D. *Science* **2015**, *347*, 522-525.

(56) Tress, W.; Marinova, N.; Moehl, T.; Zakeeruddin, S. M.; Nazeeruddin, M. K.; Grätzel, M. *Energy Environ. Sci.* **2015**, *8*, 995-1004.

(57) Xiao, Z.; Yuan, Y.; Shao, Y.; Wang, Q.; Dong, Q.; Bi, C.; Sharma, P.; Gruverman, A.; Huang, J. *Nat. Mater.* **2014**, *14*, 193-198.

(58) Sanchez, R. S.; Gonzalez-Pedro, V.; Lee, J.; Park, N.; Kang, Y. S.; Mora-Sero, I.; Bisquert, J. *J. Phys. Chem. Lett.* **2014**, *5*, 2357-2363.

(59) Li, X.; Tschumi, M.; Han, H.; Babkair, S. S.; Alzubaydi, R. A.; Ansari, A. A.; Habib, S. S.; Nazeeruddin, M. K.; Zakeeruddin, S. M.; Grätzel, M. *Energy Technology* **2015**, *3*, 551–555.

(60) Cao, K.; Cui, J.; Zhang, H.; Li, H.; Song, J.; Shen, Y.; Cheng, Y.; Wang, M. *J. Mater. Chem. A* **2015**, *3*, 9116-9122.

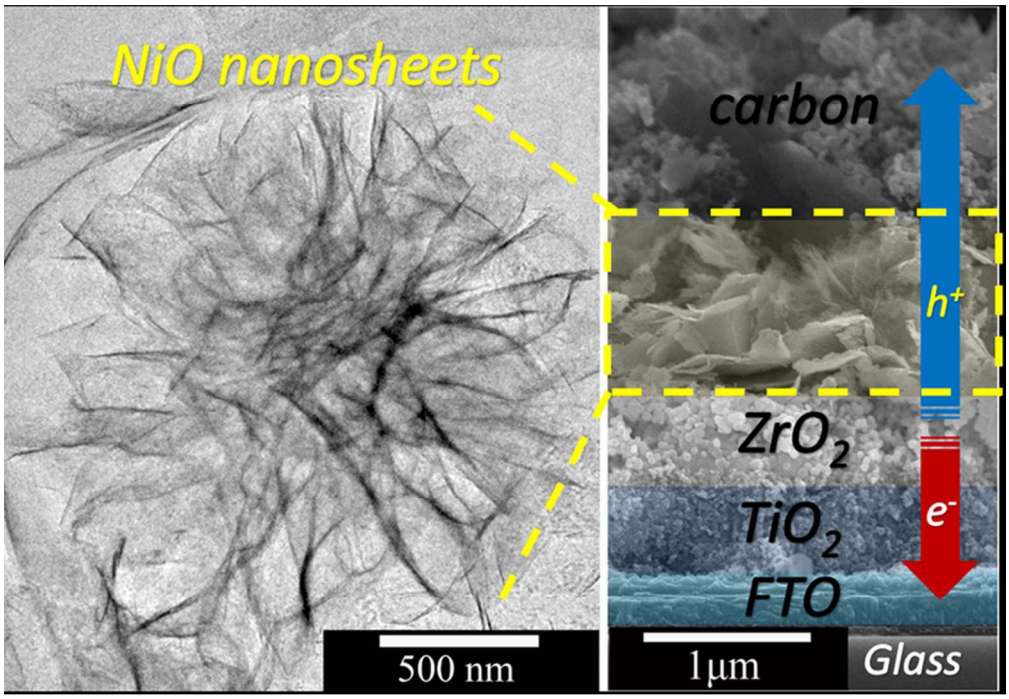

68x47mm (300 x 300 DPI)